N91-17083

A COMPARISON OF OPERATIONALLY DETERMINED ATMOSPHERIC DENSITIES FROM SATELLITE ORBIT SOLUTIONS AND THE EXOSPHERIC TEMPERATURE FROM THE JACCHIA-ROBERTS MODEL*

D. T. Ward, E. A. Smith, and M. C. Phenneger
Computer Sciences Corporation (CSC)

ABSTRACT

Operational orbit determination by the Flight Dynamics Division at the Goddard Space Flight Center has yielded a data base of orbit solutions covering the onset of solar cycle 22. Solutions for nine satellites include an estimated drag adjustment parameter (ϱ_1) determined by the Goddard Trajectory Determination System (GTDS). The ϱ_1 is used to evaluate correlations between density variations and changes in the following: 10.7-centimeter wavelength solar flux ($F_{10.7}$), the geomagnetic index A_p, and two exospheric temperatures (T_c and T_∞) adapted from the Jacchia-Roberts atmospheric density model in GTDS. T_c depends on the daily and 81-day centered mean $F_{10.7}$; T_∞ depends on T_c and the geomagnetic index K_p values. The highest correlations are between density and T_∞. Correlations with T_c and $F_{10.7}$ are lower by 9 and 10 percent, respectively. For most cases, correlations with A_p are considerably lower; however, significant correlations with A_p were found for some high-inclination, moderate-altitude orbits.

Results from this analysis enhance the understanding of the drag model and the accommodation of atmospheric density variations in the operational orbit determination support. The degree of correlation demonstrates the sensitivity of the orbit determination process to drag variations and to the input parameters that characterize aspects of the atmospheric density model. To this extent, the degree of correlation provides a measure of performance for methods of selecting or modeling the thermospheric densities using the solar $F_{10.7}$ and geomagnetic data as input to the process.

*This work was supported by the National Aeronautics and Space Administration (NASA)/Goddard Space Flight Center (GSFC), Greenbelt, Maryland, Contract NAS 5-31500.

1. INTRODUCTION

Operational orbit determination by the Flight Dynamics Division (FDD) of the Goddard Space Flight Center (GSFC) using the Goddard Trajectory Determination System (GTDS) provides routine estimates of atmospheric density. This paper uses the atmospheric drag data derived from the estimated atmospheric density scaling parameters for the following nine satellites: Dynamics Explorer (DE)-1, Earth Radiation Budget Satellite (ERBS), Landsat-4 and -5, Nimbus-7, National Oceanic and Atmospheric Administration (NOAA)-9 and -10, Solar Maximum Mission (SMM), and Solar Mesosphere Explorer (SME). The study period extends from January 1, 1988, to August 31, 1989, and covers the onset of solar cycle 22. Each orbit solution is a seven-parameter orbital state vector consisting of position and velocity vectors and an atmospheric density scaling parameter, ϱ_1. ϱ_1 is estimated to accommodate differences between modeled and actual atmospheric density and corresponding drag effects. Data for three of the nine satellites cover the early study period. Data for the other satellites became available when drag forces became large enough to provide reliable estimates of ϱ_1.

The combined data bases of ϱ_1 solutions are analyzed to evaluate correlations between density variations and changes in the following parameters, which are associated with atmospheric density modeling: 10.7-centimeter (2800 megahertz (MHz)) wavelength solar flux ($F_{10.7}$), geomagnetic index A_p, and two exospheric temperatures adapted from the Jacchia-Roberts (JR) 1971 atmospheric density model as used in GTDS (References 1 and 2). The first exospheric temperature, T_c, includes the contributions from daily $F_{10.7}$ and a centered 81-day mean, $\bar{F}_{10.7}$. The second adjusted exospheric temperature, T_∞, includes the contribution from the 3-hourly geomagnetic index K_p. Earlier work included only $F_{10.7}$ and A_p correlations with density data estimates for ERBS and SMM (Reference 3).

When data from several satellite orbits are compared, the effect of orbital geometry, altitude, and orbit solution accuracy on density correlations with solar-geomagnetic activity can be assessed. In particular, the results offer a method of assessment of the merits of using the Harris-Priester (HP) (References 4 through 6) or the JR atmospheric density model options available in GTDS without requiring extensive reprocessing of the orbit solutions using the JR model. Operational requirements to implement the JR model are now being assessed.

This paper is organized as follows. Section 2 discusses solar and geomagnetic activity, the HP and JR density models, and methods of density determination. Section 3 provides the results for each satellite, including an overview of the satellite orbit and satellite-specific operational orbit support. Section 4 provides conclusions and recommendations for further study. *NOTE*: Figures are included at the end of the text pages.

2. BACKGROUND AND PROCEDURES

The equivalent atmospheric densities are derived from the estimated ϱ_1. The absolute accuracy of this density is subject to errors in the spacecraft ballistic coefficient, but the variations in these densities relative to each other are expected to be accurate. The analysis is sensitive only to variations in the average ballistic coefficient over time intervals of 1 to 5 days, which are expected to be small.

ϱ_1 variations are caused by variations in atmospheric density driven by solar and geomagnetic activity in addition to tracking errors, geopotential modeling errors, spacecraft drag coefficient (C_D) variations, and effective cross-sectional area (A) errors. The degree to which the density variations are not correlated with the solar and geomagnetic effects is a measure of the influence of these additional factors.

A brief explanation of solar and geomagnetic parameters and their relationship to atmospheric density for the HP and JR models follows.

2.1 SOLAR-GEOMAGNETIC PHENOMENA

$F_{10.7}$ is a daily measure of solar activity and is used as an indicator of the intensity of extreme ultraviolet (EUV) radiation of the Sun, which heats the thermosphere. The degree of the correlation of $F_{10.7}$ to

EUV flux is high, except for the minimum phase of the 11-year cycle (Reference 7). The last solar minimum occurred in September 1986, when the monthly mean $F_{10.7}$ was 68.7 x 10^{-22} W m^{-2} Hz^{-1}. The $F_{10.7}$ values for this study were obtained from the National Geophysical Data Center of the Solar-Terrestrial Physics Division in Boulder, Colorado.

The 3-hourly geomagnetic index K_p is a quasi-logarithmic measurement of the geomagnetic field activity at geomagnetic latitude 50 degrees (deg) (Reference 8). The K_p values used in this study were obtained from the International Service of Geomagnetic Indices at the Institut fuer Geophysik, Goettingen, Federal Republic of Germany.

The "daily equivalent planetary amplitude," A_p, is derived by converting K_p values to a linear index and averaging over one day (Reference 9). The A_p values used in this study were provided by World Data Center A for Solar-Terrestrial Physics, National Oceanic and Atmospheric Administration E/GC2, 325 Broadway, Boulder, Colorado 80303.

The daily $F_{10.7}$ is characterized by variations with a period of the 27-day solar rotation and is referred to in the literature as the rotational component of the solar flux. The centered 81-day average, $\bar{F}_{10.7}$, is associated with clear-disk solar radiance (Reference 10). The geomagnetic indices are characterized by short, intense bursts at various intervals. A_p, $F_{10.7}$, and $\bar{F}_{10.7}$ for the 20-month period under study are shown in Figure 1.

2.2 THE HARRIS-PRIESTER DENSITY MODEL

The modified HP atmospheric density model is a set of 10 tables of atmospheric density versus altitude corresponding to ten $F_{10.7}$ levels. An atmospheric density scale factor (ϱ_1) is estimated in the differential correction (DC) solution to accommodate variations relative to the modeled drag using a selected HP table.

The acceleration due to drag, a_D, at a point in time, is given by

$$a_D = \frac{-C_D A v^2 \varrho_0 (1+\varrho_1)}{2m}$$

where m is the spacecraft mass, v is the spacecraft velocity, and ϱ_0 is the density computed from the HP tables. ϱ_0 is dependent upon the altitude, z, and the $F_{10.7}$ HP level, F_i. ϱ_0 is given by

$$\varrho_0 (z, F_i, \phi, n) = \varrho_{min} (z, F_i) + (\varrho_{max} (z, F_i) - \varrho_{min}(z, F_i)) \cos^n \left(\frac{\phi}{2}\right)$$

where ϕ is the angle between the spacecraft position and the apex of the bulge, n is an adjustable exponent, ϱ_{min} is the minimum density, and ϱ_{max} is the maximum density (References 11 and 12). Conventionally, n = 2 is used for equatorial orbits, and n = 6 is used for polar orbits. The average ϱ_0 is calculated by integrating over all ϕ.

$$\varrho_0 (z, F_i) = \frac{1}{\pi} \int_0^{\pi} \varrho_0 (z, F_i, \phi, n)\, d\phi$$

Using this ϱ_0 and the ϱ_1 estimated in the orbit solution, an equivalent density, $\varrho (z_J)$, can be determined by the following equation for each satellite orbit solution.

$$\varrho_0 (z_J) = \varrho_0 (z_J, F_i) [1 + \varrho_1 (F_i)]$$

The equivalent densities are calculated at a single HP tabulated altitude, z_J, for each spacecraft that has small altitude variations.

The variation in altitude for each spacecraft over the study period was much less than the atmospheric scale height, except for SMM and DE-1. To isolate changes in density that were not due to altitude, DE-1 and SMM densities were converted back to ϱ_1 (F_i), an equivalent ϱ_1 , for HP tables 7 and 4, respectively. The following equation was used for SMM:

$$\varrho_1 (F_4) = \frac{\varrho_0 (z, F_i) [1 + \varrho_1 (F_i)]}{\varrho_0 (z, F_4)} - 1,$$

where ϱ_0 (z, F_i) is determined using exponential scale heights from HP tables.

2.3 JACCHIA-ROBERTS DENSITY MODEL AND EXOSPHERIC TEMPERATURES

The Jacchia-Roberts 1971 (JR71) atmospheric density model option in GTDS gives the density at a given altitude from the $F_{10.7}$, $\bar{F}_{10.7}$, and K_p input data. In the JR71 model, the nighttime minimum global exospheric temperature for zero geomagnetic activity (T_c) is computed from the daily $F_{10.7}$ and the 81-day mean $\bar{F}_{10.7}$, as follows (Reference 12):

$$T_c = 379° + 3.24° \bar{F}_{10.7} + 1.3° (F_{10.7} - \bar{F}_{10.7})$$

There is an approximate 1-day lag (Reference 13) between solar flux change and a resulting change in exospheric temperature.

For simplicity in this work, a geometrical factor, which varies T_c with spacecraft geodetic latitude and the solar declination, was not accounted for in determining exospheric temperature T_∞. The variation in the amplitude of this factor over a season is 30 percent of T_c , but it is averaged over many orbits and is not tested in the correlations that were much shorter than the seasonal variation.

The correction to the exospheric temperature for geomagnetic activity is

$$\Delta T_\infty = 28°.0 K_p + 0°.03 \exp (K_p)$$

The corrected exospheric temperature used here is

$$T_\infty = T_c + \Delta T_\infty$$

For a 6.7-hour lag in the response to K_p (Reference 12), T_c and T_∞ are illustrated in Figure 2.

3. DENSITY DATA AND RESULTS

Tables 1a and 1b provide background information on the satellites studied. Table 1a provides the average data arc length and the orbital parameters: altitude, eccentricity, and inclination. Table 1b provides the GTDS modeling characteristics: C_D, A, mass, diurnal bulge model, and the maximum order and degree of the Goddard Earth Model (GEM)-9 geopotential model matrix.

The standard solution tracking data arc length varies by several hours due to the granularity of the tracking schedule. The $F_{10.7}$, A_p, T_c , and T_∞ data were averaged for each satellite over the average tracking

Table 1a. Average Data Arc Lengths and Orbital Parameters

Spacecraft	Average Data Arc Length	Altitude (km)	Eccentricity	Inclination (deg)
DE-1	3 days, 4.40 hours	470 to 23,350	0.62	89.2
ERBS	5 days, 6.62 hours 4 days, 6.62 hours	600	0.0005	57.
Landsat-4	1 day, 3.09 hours	700	0.0003	98.2
Landsat-5	1 day, 2.54 hours	700	0.0003	98.2
Nimbus-7	3 days, 8.79 hours	950	0.0009	99.2
NOAA-9	7 days, 0.00 hour	850	0.0015	99.1
NOAA-10	7 days, 0.00 hour	813	0.0014	98.6
SMM	2 days, 7 hours, 1 day, 7 hours	485 to 390	0.0002	28.5
SME	2 days, 14.54 hours	503 to 482	0.0002	97.7

5841G(4)-2a

Table 1b. GTDS Modeling Characteristics

Spacecraft	C_D	A (m^2)	Mass (kg)	Bulge	GEM-9
DE-1	2.3	3.05	402.79005	$\cos^6$	16 x 16
ERBS	2.2	4.7	2116.	$\cos^2$	8 x 8
Landsat-4	2.2	12.2644	1932.2669	$\cos^6$	21 x 21
Landsat-5	2.2	12.664	1943.538	$\cos^6$	21 x 21
Nimbus-7	2.1	9.5597	938.03	$\cos^6$	8 x 8
NOAA-9	2.3	10.79	1029.3	$\cos^6$	8 x 8
NOAA-10	2.3	10.79	1029.3	$\cos^6$	8 x 8
SMM	2.2	17.5	2315.59	$\cos^2$	16 x 16
SME	2.3	1.129	415.5	$\cos^6$	21 x 21

5841G(4)-2b

arc to be consistent with the density parameters estimated for the tracking arc. Correlation analysis results for each spacecraft are presented in the following sections. The correlation coefficients (r) from linear regressions are summarized in Table 2.

3.1 DYNAMICS EXPLORER-1

DE-1 is unique among the satellites studied because of its high eccentricity orbit. The DE-1 orbit is affected by atmospheric drag primarily near perigee. Operational estimation of ϱ_1 began on November 12, 1988. The equivalent ϱ_1 values were calculated using the HP table 7 and the DE-1 altitude perigee. These values are plotted versus epoch in Figure 3a. The correlations of these data with

Table 2. Correlation Coefficients Analysis

Spacecraft	No. of Epochs	Density Correlation Coefficients			
		$F_{10.7}$	T_c	T_∞	A_p
DE-1	148	0.36	0.30	0.50	0.58
ERBS	172	0.87	0.88	0.90	0.41
Landsat-4	351	0.48	0.50	0.67	0.68
Landsat-5	344	0.51	0.55	0.70	0.68
Nimbus-7	132	0.47	0.39	0.57	0.72
NOAA-9	65	0.76	0.79	0.83	0.52
NOAA-10	65	0.75	0.80	0.84	0.55
SMM	412	0.83	0.85	0.88	0.40
SME	234	0.83	0.86	0.90	0.52

5841G(4)-1

$F_{10.7}$, T_c, T_∞, and A_p are shown in Figures 3b, 3c, 3d, and 3e, respectively. The highest equivalent ϱ_1 corresponds to an extreme geomagnetic storm on March 13, 1989. A large increase in T_∞ and T_c occurred in early December 1988 due to rapidly rising $F_{10.7}$, evidenced by clumping or gaps in ϱ_1 versus temperature in Figures 3c and 3d. The low correlation of ϱ_1 with solar and geophysical parameters demonstrates that the measurability of density is small for DE-1. At each perigee passage the satellite samples many different altitudes. During the study period the perigee height decreased from 570 to 470 km while the perifocal latitude decreased from 80-deg N to 20-deg N. Recent operational work has shown that a more consistent ϱ_1 is estimated using a 21 x 21 GEM-9 model. An improvement of 0.05 in the correlation coefficients for the $F_{10.7}$, T_c, and T_∞ relations occurred when an equivalent ϱ_1 was used in place of an equivalent density. The two densities are compared in Figure 3f.

3.2 EARTH RADIATION BUDGET SATELLITE

Operational estimates of ϱ_1 for ERBS have been made since launch in 1984. Data from launch through October 31, 1987, were analyzed in Reference 3. The equivalent densities for ERBS were calculated with the HP altitude of 600 km. These are plotted versus epoch in Figure 4a. The correlations of these data with $F_{10.7}$, T_c, T_∞, and A_p are illustrated in Figures 4b, 4c, 4d, and 4e, respectively. Except for r_{A_p}, these correlations are high, with $r_{T_\infty} = 0.90$. The low A_p correlation corresponds to the averaging reduction of those short-term phenomena by orbit estimation over long tracking data arcs. Corresponding Jacchia 1977 (J77) density-temperature models (Reference 14), with a nonlinear curvature similar to that in Figure 4d, have a linear correlation coefficient of 0.94. Figure 4d includes the J77 densities corresponding to the average exospheric temperatures over the ERBS solution arcs. A polynomial fit was used to determine the density-temperature relationship in the J77 model at ERBS's altitude. After converting each average temperature to a J77 density, the J77 densities were correlated with the equivalent densities. A zero-intercept linear regression of the two densities yielded a scale factor of 2.4 for the J77 densities to best match the equivalent densities. The scaled J77 density curve is plotted in Figure 4d.

Previous work for low levels of solar activity (October 1984 to October 1987) found $r_{F_{10.7}} = 0.24$ and $r_{Ap} = 0.56$, using values averaged over the solution days, without time lags. Current $F_{10.7}$ correlations are significantly higher. This is not surprising, since the previous work included data only during the solar minimum. The greatly increased density levels allow a far more reliable density estimation.

3.3 LANDSAT-4 AND -5

Operational estimates of ϱ_1 for Landsat-4 began on July 1, 1988. The equivalent densities were calculated using the HP altitude of 700 km. These are plotted versus epoch in Figure 5a. For the first few months, ϱ_1 determinations were made only near solar flux peaks. The correlations of density with $F_{10.7}$, T_c, T_∞, and A_p are illustrated in Figures 5b, 5c, 5d, and 5e. Figure 5d includes a J77 density curve, described above, with a scale factor of 4.70. The correlations of density with $F_{10.7}$, T_c, and T_∞ are lower for Landsat-4, with r_{T_∞} the highest at 0.67. The A_p correlation is 0.68, which reflects the high inclination orbit sensitivity that is enhanced by the shorter solution arc. Note the improvement in correlation with T_∞ for the highest density point, corresponding to the March 13, 1989, geomagnetic storm.

It has been demonstrated that errors in the geopotential model affect the determination of ϱ_1 for Landsat-4 (Reference 15). These may contribute to the low Landsat correlation coefficients. An attempt to remove these errors for Landsat-4 was made by averaging densities and corresponding solar-geophysical parameter values over a 5-day interval, which is near two beat periods of the Landsat orbital resonance with 15th-order geopotential harmonics. No change in correlation coefficients was observed.

The density and correlations plots for Landsat-5 are not pictured. They are nearly identical to Landsat-4. Landsat-5 equivalent densities are plotted versus Landsat-4 equivalent densities in Figure 5f.

3.4 NIMBUS-7

Operational estimates of ϱ_1 for Nimbus-7 began in October 1988. The equivalent density data for Nimbus-7 were calculated using the HP altitude of 950 km. These are plotted against epoch in Figure 6a. The correlations of these densities with $F_{10.7}$, T_c, T_∞, and A_p are illustrated in Figures 6b, 6c, 6d, and 6e, respectively. The correlations are low for Nimbus-7, with r_{A_p} the highest at 0.72. This highest r_{A_p} corresponds to the highest altitude, and high inclination. The low value of r_{T_∞} may be due to the truncation of the geopotential model but also indicates that density is less measurable at that altitude.

3.5 NOAA-9 AND -10

Operational estimates of ϱ_1 for NOAA-9 and -10 have been performed since June 1988. The equivalent densities for NOAA-9 and -10 were calculated using HP altitudes of 850 and 800 km, respectively. These are plotted versus epoch in Figures 7a. The correlations of these densities with $F_{10.7}$, T_c, T_∞, and A_p are illustrated in Figures 7b, 7c, 7d, and 7e. The correlations of density to $F_{10.7}$, T_c, and T_∞ for NOAA-9 and -10 are high, with r_{T_∞} = 0.83 and 0.84, respectively. This correlation is more pronounced than that for Landsat-4 and Landsat-5 described in a previous section. Landsat-4 and Landsat-5 are at lower altitudes and use shorter tracking data arcs. This result demonstrates that drag perturbations are better measured using long tracking data arcs. Lower r_{A_p} for these spacecraft are a result of an increased tracking arc length. NOAA-9 density is plotted versus NOAA-10 density in Figure 7f.

3.6 SOLAR MAXIMUM MISSION

SMM was launched February 14, 1980, and reentered on December 2, 1989. Daily orbit solutions were performed after January 27, 1989. Before that, orbit solutions were performed every other day. The equivalent ϱ_1 relative to HP table 4 (to remove altitude-dependent variations) are illustrated in Figure 8a. The correlations of ϱ_1 with $F_{10.7}$, T_c, T_∞, and A_p are illustrated in Figures 8b, 8c, 8d, and 8e, respectively. The correlations of density to $F_{10.7}$, T_c, and T_∞ are high for SMM, with r_{T_∞} = 0.88 being the highest. Thus, the acceleration due to drag is dominating the solutions, as expected. This lowest r_{A_p} corresponds to the lowest altitude and inclination of the group. Previous results from launch to October 1987 were comparable to current results, with $r_{F_{10.7}}$ = 0.86 and r_{A_p} = 0.25 (Reference 3).

3.7 SOLAR MESOSPHERE EXPLORER

Operational estimates of ϱ_1 were performed for SME until contact with the spacecraft was lost on April 14, 1989. The equivalent densities for SME were calculated using the HP altitude of 500 km.

These are plotted versus epoch in Figure 9a. The correlations of density to $F_{10.7}$, T_c, T_∞, and A_p are shown in Figures 9b, 9c, 9d, and 9e, respectively. The correlations of the data with $F_{10.7}$, T_c, and T_∞ are high for SME, with $r_{T_\infty} = 0.90$ being the highest. SME's low altitude and polar orbit thus cause more sensitivity to solar and geomagnetic activity, respectively. The low r_{A_p} corresponds to low altitude and a moderate tracking data arc length.

4. CONCLUSIONS AND RECOMMENDATIONS

The operational data base of estimated ϱ_1 values for nearly 2 years of orbit solutions has been presented. Correlations of estimated atmospheric density with solar and geomagnetic activity measurements have been evaluated. The highest correlations were with the exospheric temperature T_∞, adapted from the JR71 model. T_∞ includes a dependence on the daily $F_{10.7}$, 81-day mean $\bar{F}_{10.7}$, and on 3-hourly K_p values. Lower altitude spacecraft (ERBS, SME, and SMM) densities correlate best with T_∞, T_c, and $F_{10.7}$, due to the larger drag at lower altitudes. At higher altitudes, longer arc solutions had correlations nearly as high as the low-altitude solutions. The correlation of density with T_∞ in each case is discernibly higher than with T_c or $F_{10.7}$, showing that the K_p correction improves the correlations more than does the $\bar{F}_{10.7}$ component.

A_p affects estimated density more at high inclinations and high altitudes than it does at low inclinations and low altitudes. Shorter arcs are more sensitive to A_p. The degree of correlation with A_p is highest during severe geomagnetic storm conditions. A_p, which accounts for the largest deviations in the T_c and the $F_{10.7}$ correlations, generally has a low correlation with density, except for Nimbus-7 and the Landsats.

Lack of higher correlations for the Landsats may be a result of short arc lengths or orbit modeling errors due to resonance with geopotential harmonic coefficients of the 15th order and degree. The low correlations for DE-1 arise because its orbit solution is the least affected by atmospheric drag.

Jacchia-Roberts modeling of exospheric temperature T_∞ is a better monitor of variations in atmospheric density than T_c, $F_{10.7}$, or A_p. ϱ_1 estimates using the HP model reflect the additional physical processes that are part of the JR model but are not included in the HP model. The correlations of density with solar-geomagnetic activity shown in this paper can be used to improve the use of the HP model in the predictive mode.

This paper extends the work begun in Reference 3. A large amount of data for SME from launch in 1981 to January 1988 has not been used. Other data during the previous solar maximum also exists for Landsat-4 and Nimbus-7. ϱ_1 estimations for most satellites were suspended during the solar minimum. Data continue to be accumulated during solar cycle 22. We recommend that these data be included in similar future analysis.

The estimation of density from satellite data is a valuable extension of operational orbit determination. The correlations evaluated here provide only a survey of the information available. Higher resolution studies concentrating on measurements of the atmospheric response time to various solar-geophysical stimuli are possible. Archived tracking data can be used to obtain density estimates over shorter or longer time intervals.

ACKNOWLEDGMENTS

The authors wish to thank Dana Peters (CSC) for her valuable contribution to the generation of a portion of these data. We also wish to thank Osvaldo Cuevas (NASA/GSFC) and Avinash Beri (CSC) for their thoughtful reviews of the draft.

REFERENCES

1. L. G. Jacchia, *Revised Static Models of the Thermosphere and Exosphere with Empirical Temperature Profiles*, Smithsonian Astrophysical Observatory Special Report No. 332, Cambridge, Massachusetts, May 1971

2. E. R. Roberts, Jr., "An Analytic Model for Upper Atmosphere Densities Based Upon Jacchia's 1970 Models," *Celestial Mechanics*, vol. 4, December 1971, pp. 368-377

3. E. A. Smith, "Correlations Between Solar Activity and Operationally Determined Satellite Drag Variation Parameters," Paper No. 27, presented at the GSFC Flight Mechanics/Estimation Theory Symposium, Greenbelt, Maryland, May 1988

4. I. Harris and W. Priester, "Time Dependent Structure of the Upper Atmosphere," *Journal of the Atmospheric Sciences*, vol. 19, July 1962, pp. 286-301 (also NASA-TN-D-1443)

5. I. Harris and W. Priester, *Theoretical Models for the Solar Cycle Variation of the Upper Atmosphere*, Goddard Space Flight Center Report NASA-TN-D-1444, August 1962

6. I. Harris and W. Priester, "Atmospheric Structure and Its Variations in the Region From 120 to 80 km," *COSPAR International Reference Atmosphere (CIRA) 1965, Space Research IV*, North Holland Publishing Company, Amsterdam, 1965

7. W. K. Tobiska, C. A. Barth, and R. D. Culp, "Use of Solar Lyman-α and 1-8 Å X-Rays as EUV Flux Indices," Paper No. 88-4293, presented at AIAA/AAS Astrodynamics Conference, Minneapolis, Minnesota, August 1988

8. Solar-Geophysical Data, 515 Supplement, July 1987, pp. 30-31, U.S. Department of Commerce (Boulder, Colorado 80303)

9. G. Rostoker, "Geomagnetic Indices," *Reviews of Geophysics and Space Physics*, vol. 10, November 1972, pp. 935-950

10. L. G. Jacchia and J. W. Slowey, "A Study of the Variations in the Thermosphere Related to Solar Activity," *Space Research XIII*, Akademie-Verlag, Berlin, 1973, pp. 343-348

11. E. A. Smith, D. T. Ward, M. W. Schmitt, M. C. Phenneger, F. J. Vaughn, and M. L. Lupisella, "Lifetime Predictions for the Solar Maximum Mission (SMM) and San Marco Spacecraft," Paper No. 27, presented at the GSFC Flight Mechanics/Estimation Theory Symposium, Greenbelt, Maryland, May 1989

12. Computer Sciences Corporation, *Goddard Trajectory Determination System Mathematical Theory (Revision 1)*, FDD/552-89/0001 and CSC/TR-89/6001, eds. A. C. Long, J. O. Cappellari, Jr., C. E. Velez, and A. J. Fuchs, July 1989

13. L. G. Jacchia, J. W. Slowey, and I. G. Campbell, "Analysis of Solar Activity Effects on the Upper Atmosphere," *Planetary and Space Science*, vol. 21, November 1973, pp. 1835-1842

14. L. G. Jacchia, *Thermospheric Temperature, Density, and Composition: New Models*, Smithsonian Astrophysical Observatory Special Report No. 375, Cambridge, Massachusetts, May 1977

15. S. L. Hoge, D. O. Casteel, M. C. Phenneger, and E. A. Smith, "The Effects of Geopotential Resonance on Orbit Determination for Landsat-4," Paper No. 88-4296, presented at AIAA/AAS Astrodynamics Conference, Minneapolis, Minnesota, August 1988

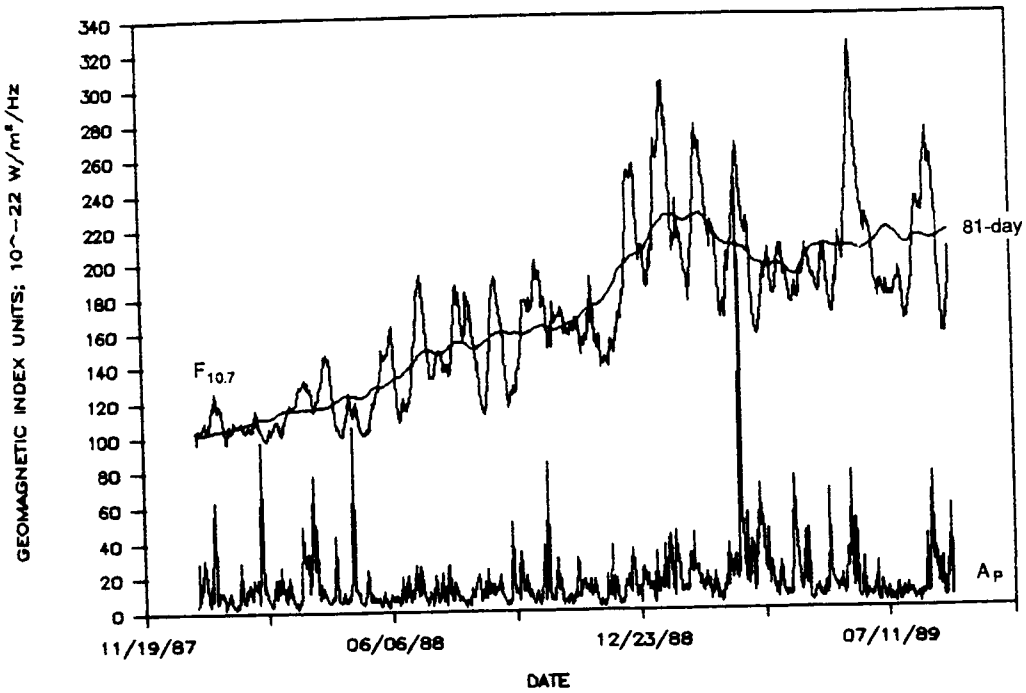

Figure 1. Daily Observed $F_{10.7}$, 81-Day Mean $\overline{F}_{10.7}$, and A_p

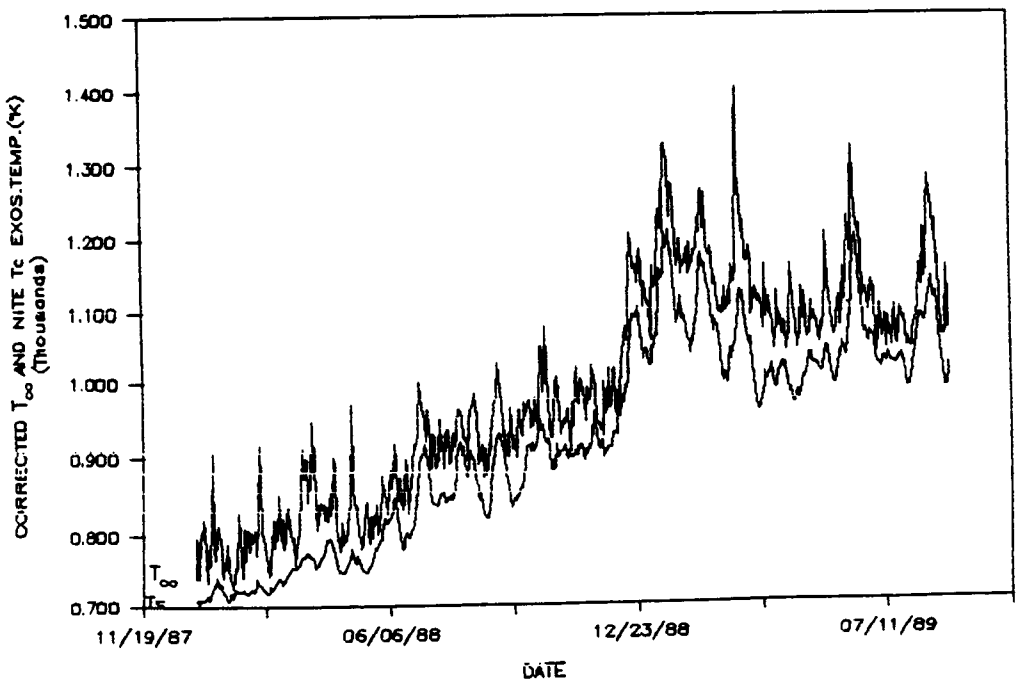

Figure 2. Daily Exospheric Temperatures, T_∞ and T_c

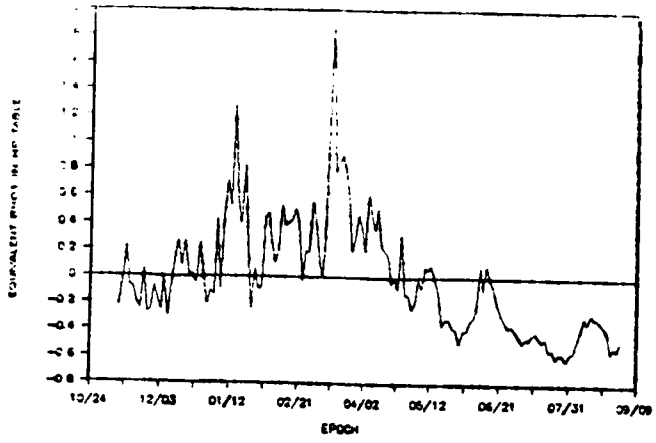

Figure 3a. DE-1 Equivalent ϱ_1 Values Versus Epoch

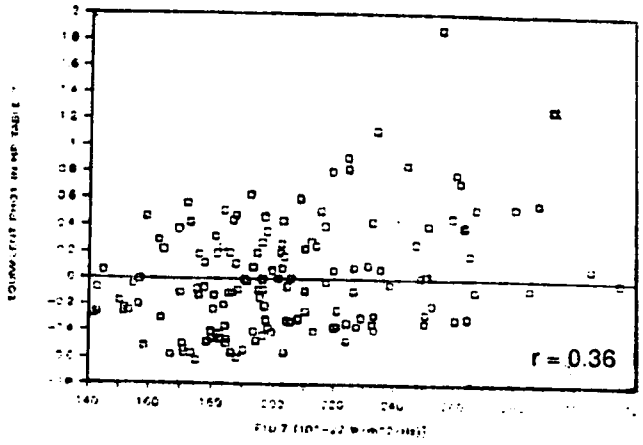

Figure 3b. DE-1 Equivalent ϱ_1 Values Versus $F_{10.7}$

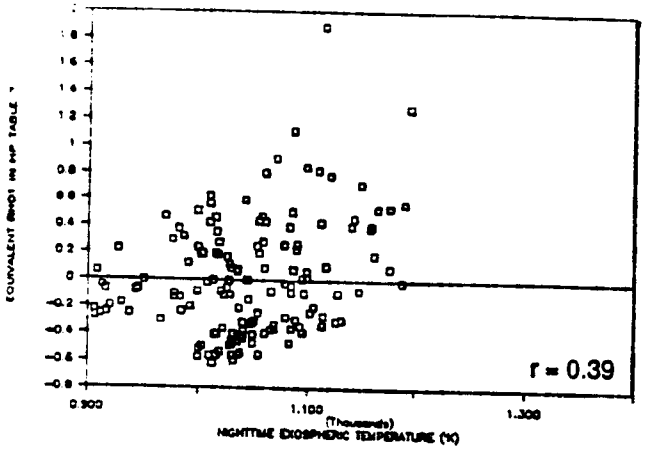

Figure 3c. DE-1 Equivalent ϱ_1 Values Versus T_c

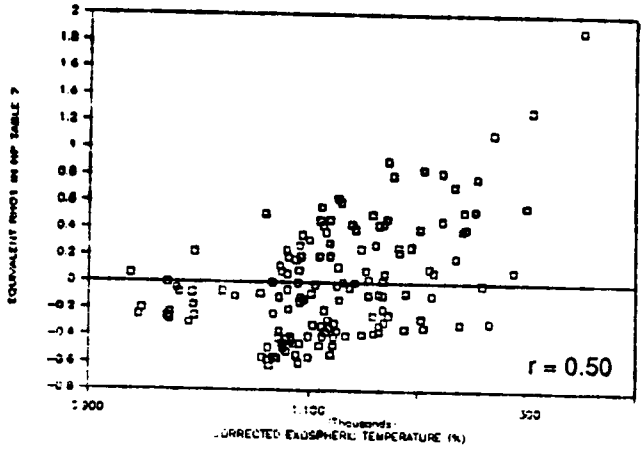

Figure 3d. DE-1 Equivalent ϱ_1 Values Versus T_∞

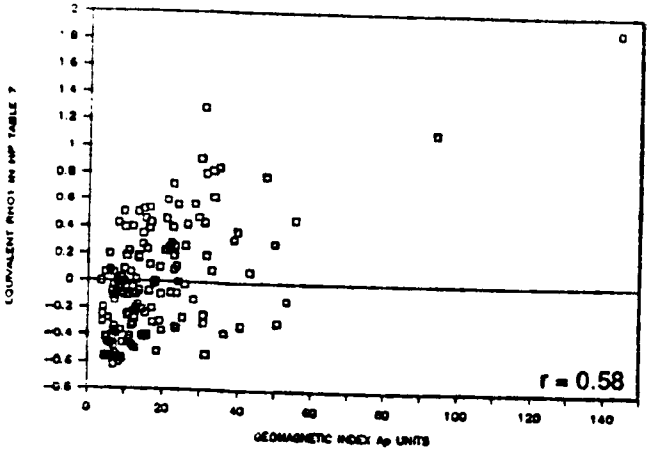

Figure 3e. DE-1 Equivalent ϱ_1 Values Versus A_p

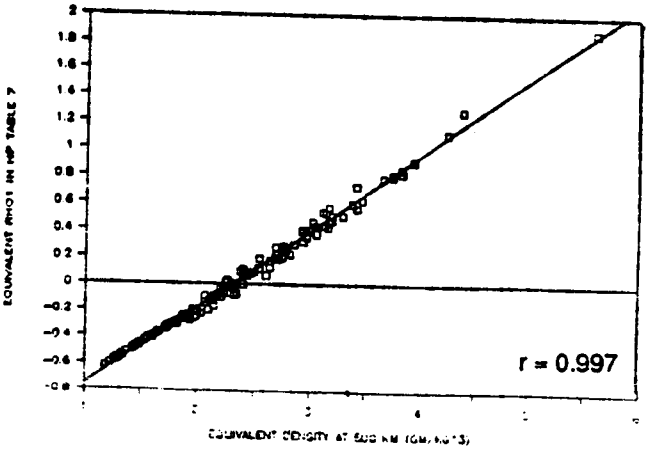

Figure 3f. DE-1 Equivalent ϱ_1 Values Versus Equivalent Density at 500 km

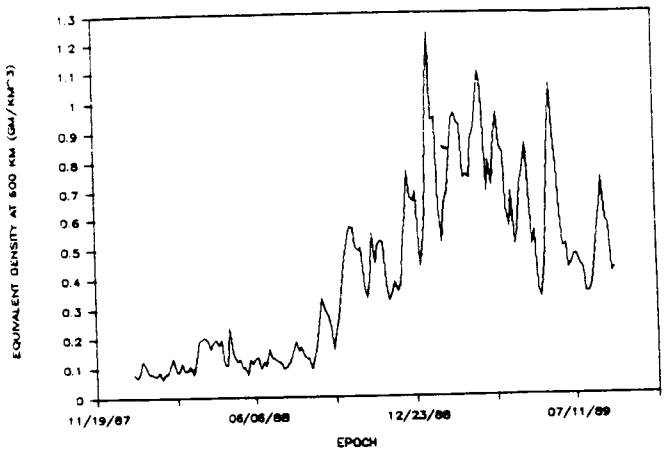

Figure 4a. ERBS Equivalent Density Versus Epoch

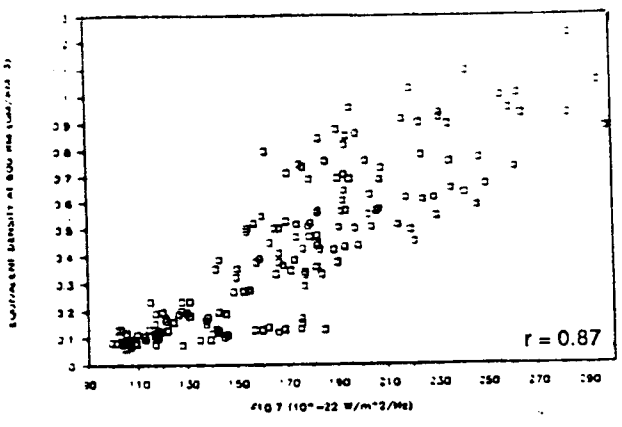

Figure 4b. ERBS Equivalent Density Versus $F_{10.7}$

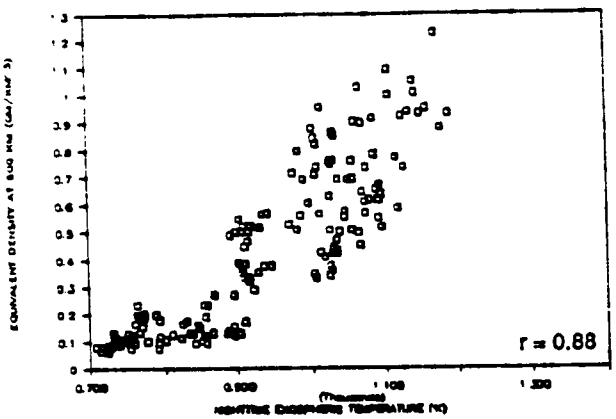

Figure 4c. ERBS Equivalent Density Versus T_c

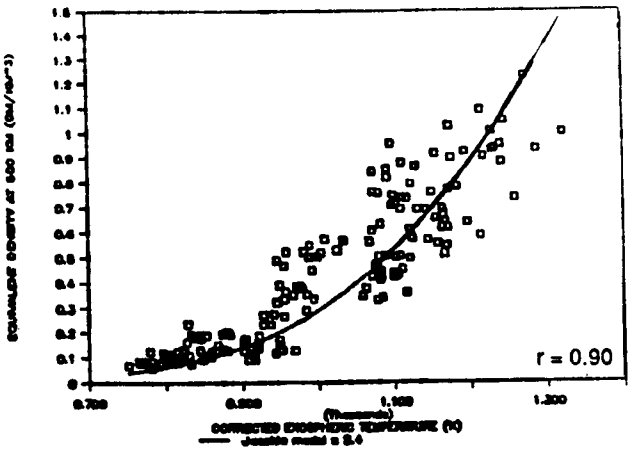

Figure 4d. ERBS Equivalent Density and Scaled Jacchia Model Versus T_∞

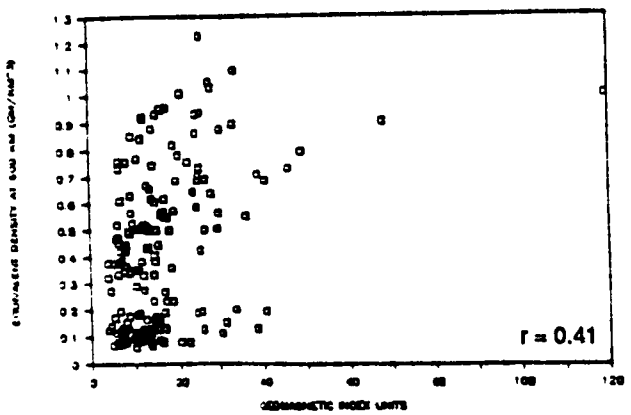

Figure 4e. ERBS Equivalent Density Versus A_p

ORIGINAL PAGE IS
OF POOR QUALITY

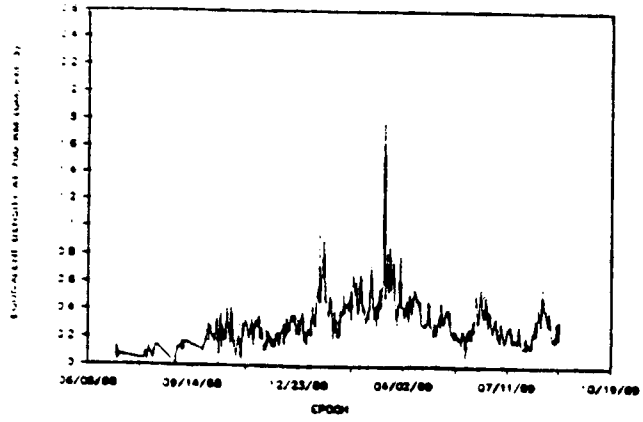

Figure 5a. Landsat-4 Equivalent Density Versus Epoch

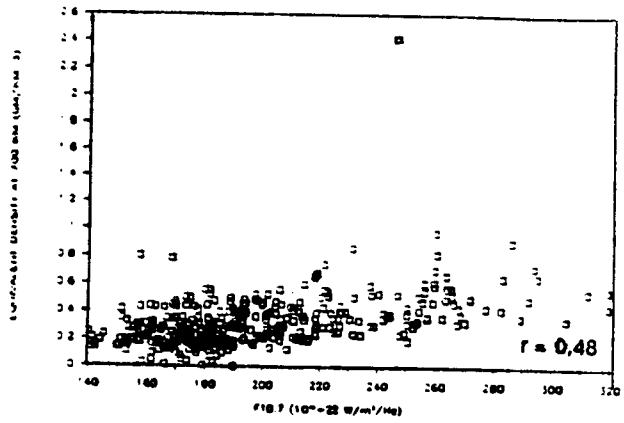

Figure 5b. Landsat-4 Equivalent Density Versus $F_{10.7}$

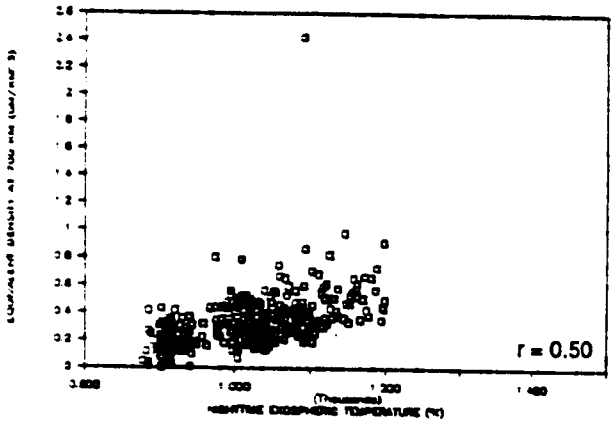

Figure 5c. Landsat-4 Equivalent Density Versus T_c

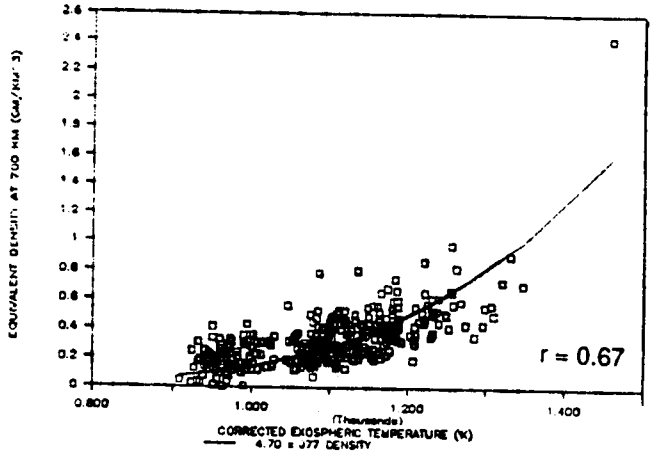

Figure 5d. Landsat-4 Equivalent Density and Scaled Jacchia Model Versus T_∞

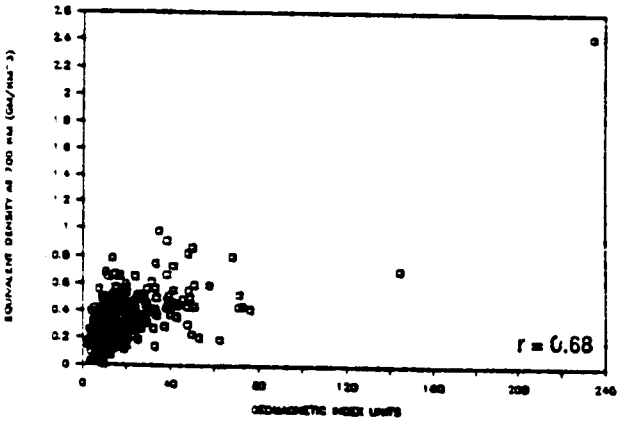

Figure 5e. Landsat-4 Equivalent Density Versus A_p

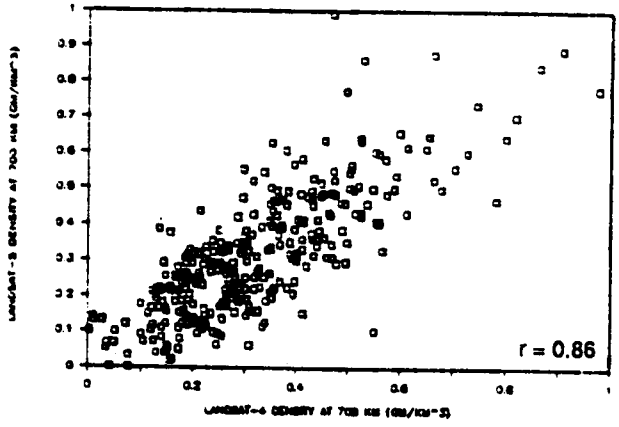

Figure 5f. Landsat-5 Equivalent Density Versus Landsat-4 Equivalent Density

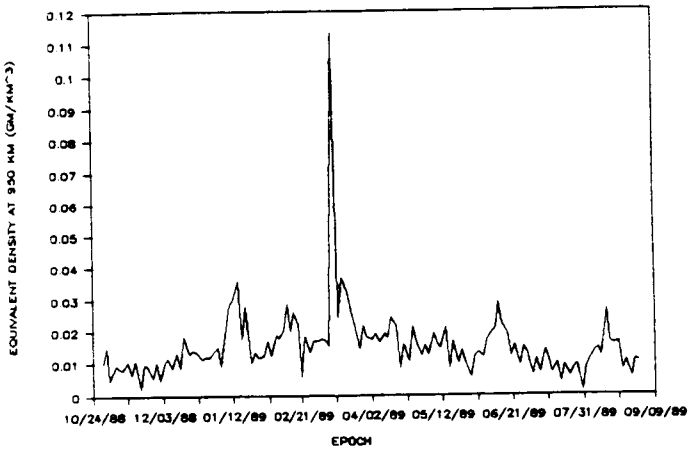

Figure 6a. Nimbus-7 Equivalent Density Versus Epoch

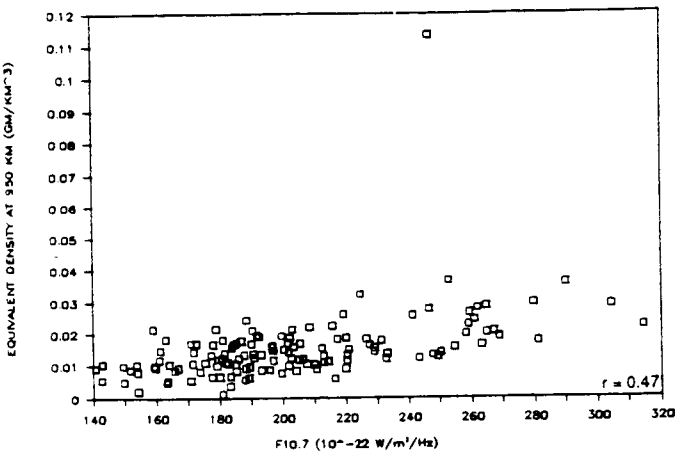

Figure 6b. Nimbus-7 Equivalent Density Versus $F_{10.7}$

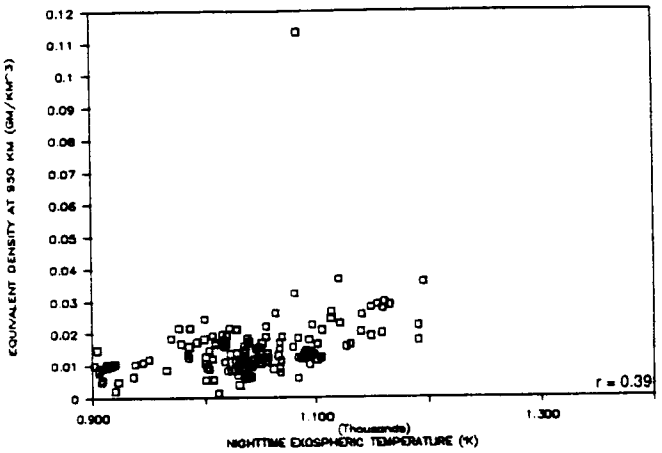

Figure 6c. Nimbus-7 Equivalent Density Versus T_c

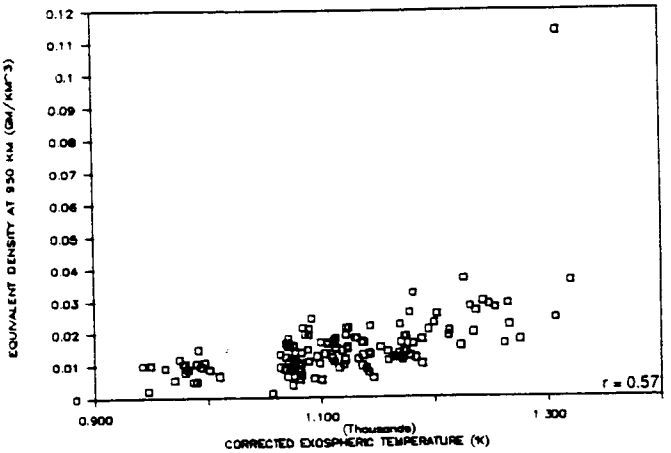

Figure 6d. Nimbus-7 Equivalent Density Versus T_∞

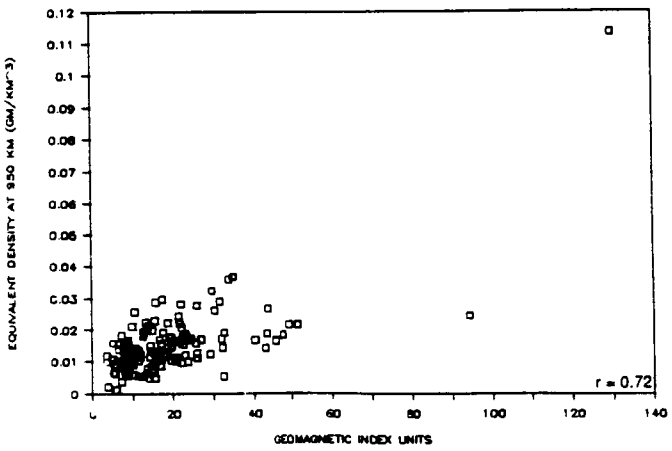

Figure 6e. Nimbus-7 Equivalent Density Versus A_p

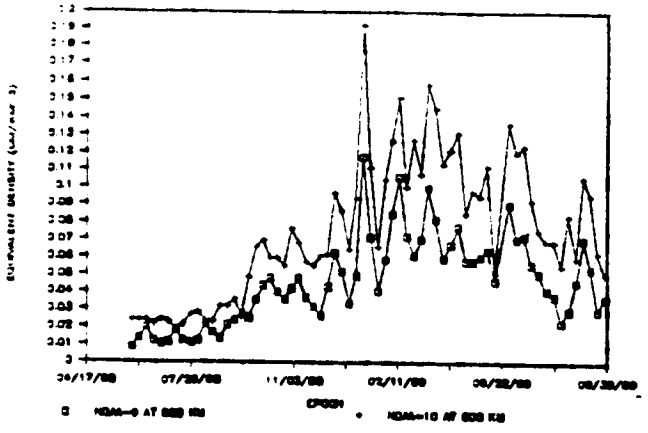

Figure 7a. NOAA-9, -10 Equivalent Density Versus Epoch

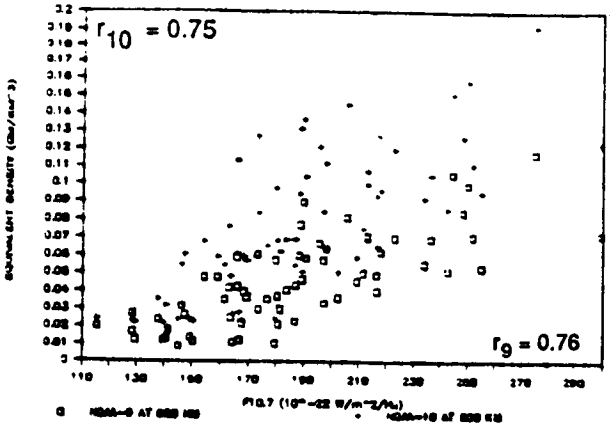

Figure 7b. NOAA-9, -10 Equivalent Density Versus $F_{10.7}$

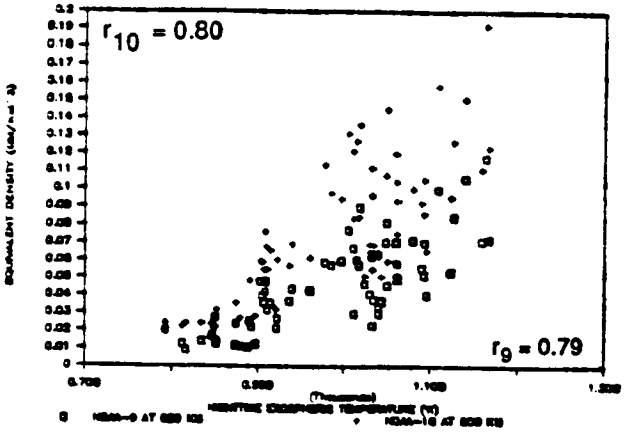

Figure 7c. NOAA-9, -10 Equivalent Density Versus T_c

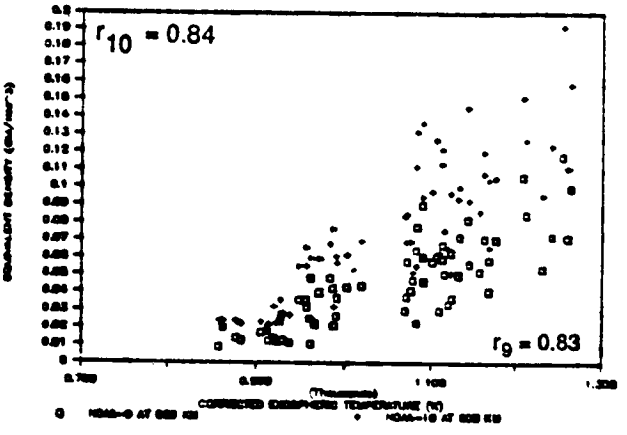

Figure 7d. NOAA-9, -10 Equivalent Density Versus T_∞

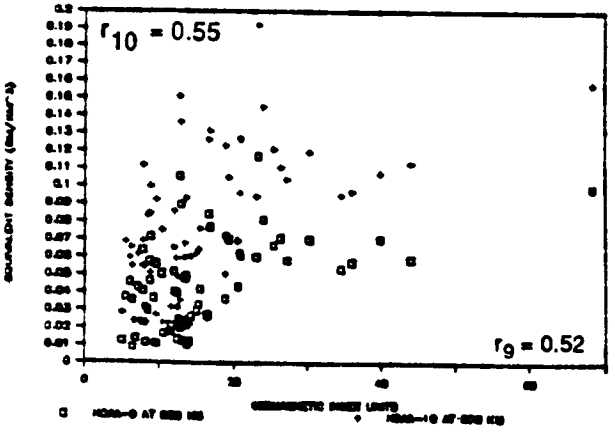

Figure 7e. NOAA-9, -10 Equivalent Density Versus A_p

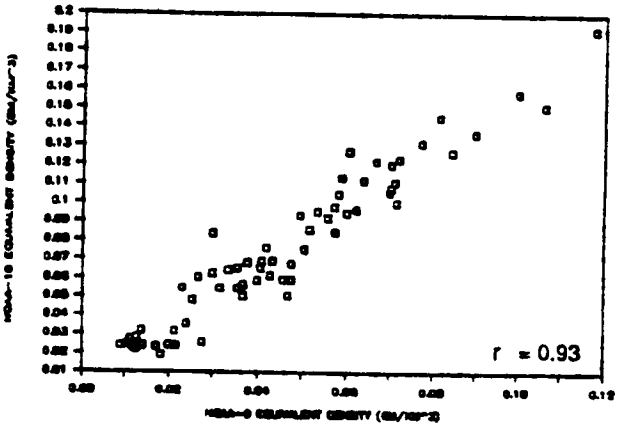

Figure 7f. NOAA-10 Equivalent Density Versus NOAA-9 Equivalent Density

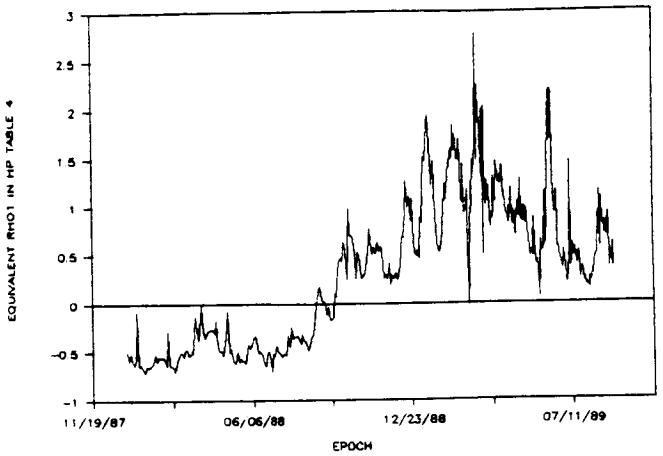

Figure 8a. SMM Equivalent ϱ_1 Values at HP 4 Versus Epoch

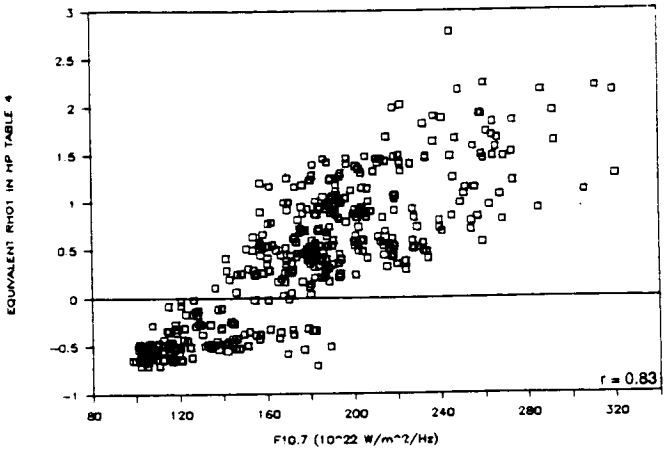

Figure 8b. SMM Equivalent ϱ_1 Values Versus $F_{10.7}$

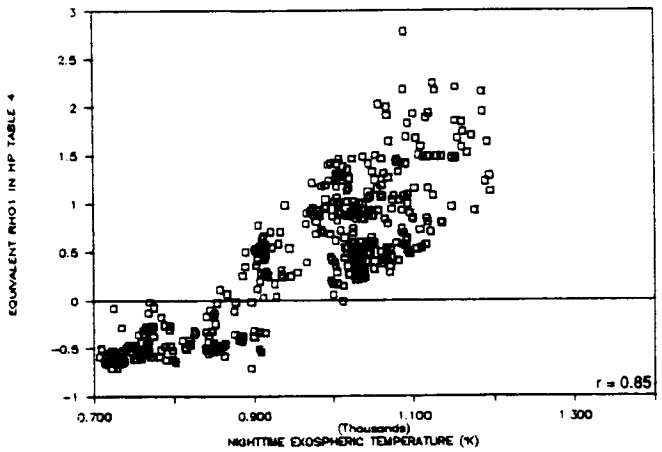

Figure 8c. SMM Equivalent ϱ_1 Values Versus T_c

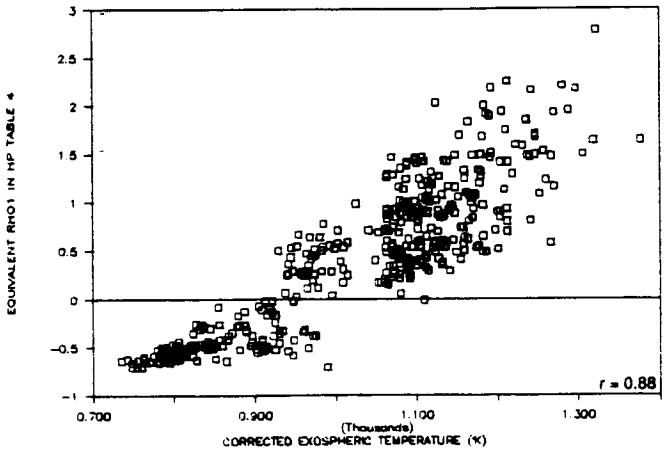

Figure 8d. SMM Equivalent ϱ_1 Values Versus T_∞

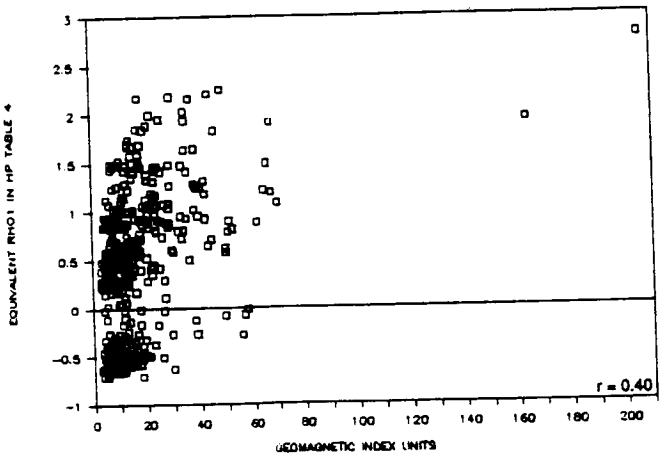

Figure 8e. SMM Equivalent ϱ_1 Values Versus A_p

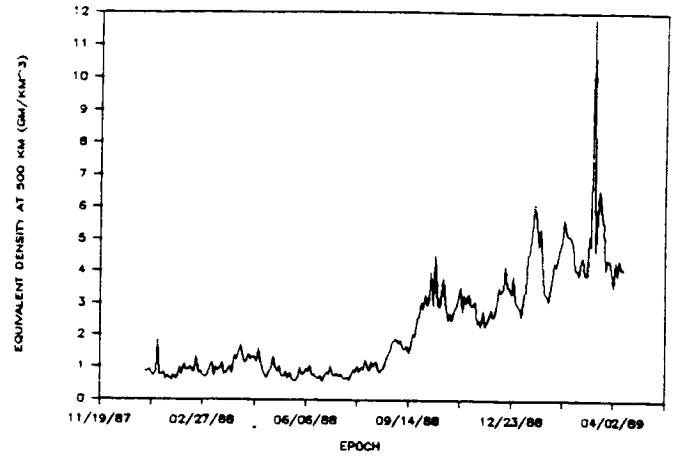

Figure 9a. SME Equivalent Density Versus Epoch

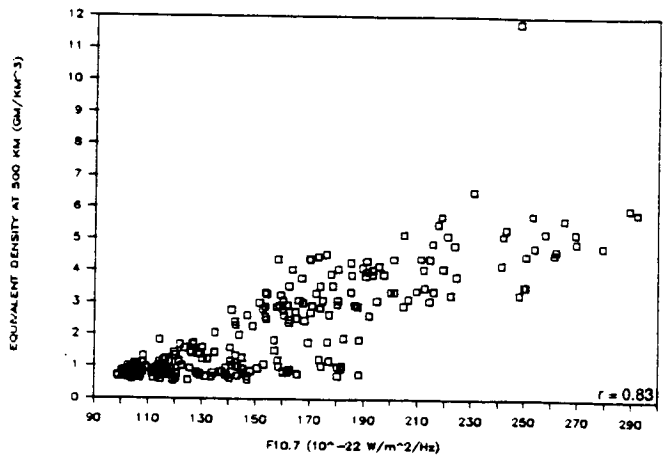

Figure 9b. SME Equivalent Density Versus $F_{10.7}$

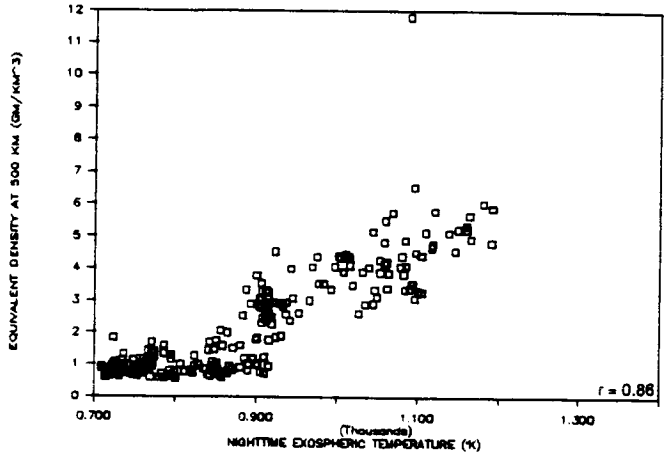

Figure 9c. SME Equivalent Density Versus T_c

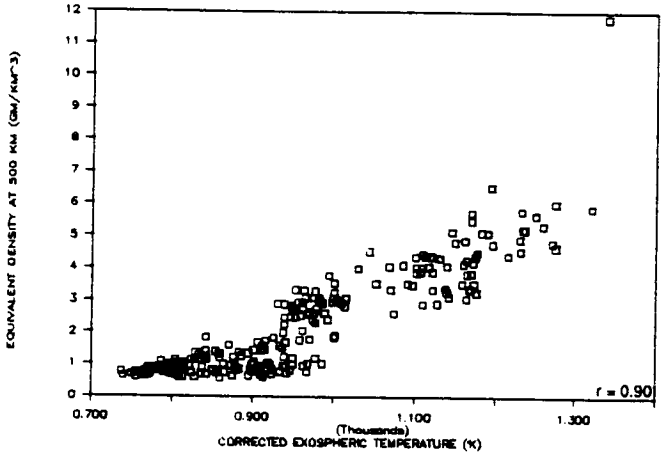

Figure 9d. SME Equivalent Density Versus T_∞

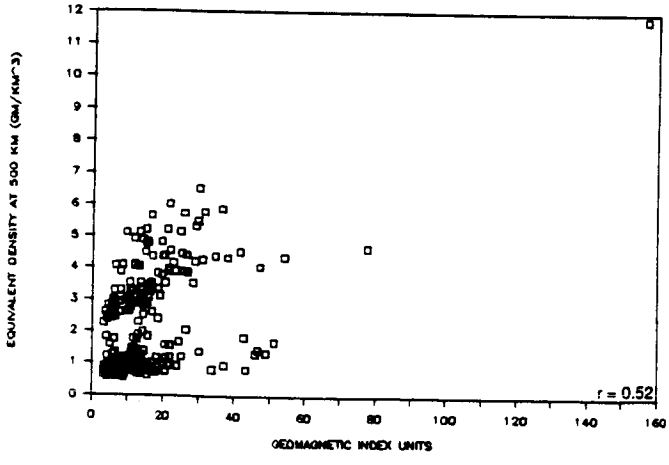

Figure 9e. SME Equivalent Density Versus A_p